

Off-nuclear H₂O maser and dense molecular gas in NGC 1068

Yoshiaki Hagiwara,^{1,2,3*} Willem A. Baan,^{2,4} Masatoshi Imanishi,^{5,6,7} and Philip Diamond⁸

¹*Natural Science Laboratory, Toyo University, 5-28-20, Hakusan, Bunkyo-ku, Tokyo 112-8606 Japan*

²*Netherlands Institute for Radio Astronomy ASTRON, 7991 PD Dwingeloo, the Netherlands*

³*Joint Institute for VLBI ERIC, 7991 PD Dwingeloo, the Netherlands*

⁴*XinJiang Astronomical Observatory, Chinese Academy of Sciences, Urumqi, PR China*

⁵*National Astronomical Observatory of Japan, National Institutes of Natural Sciences (NINS) 2-21-1 Osawa, Mitaka, Tokyo 181-8588, Japan*

⁶*Department of Astronomy, School of Science, The Graduate University for Advanced Studies, SOKENDAI 2-21-1 Osawa, Mitaka, Tokyo 181-8588 Japan*

⁷*Toyo University, 5-28-20, Hakusan, Bunkyo-ku, Tokyo 112-8606 Japan*

⁸*SKA Observatory Jodrell Bank, Lower Withington, Macclesfield, SK11 9FT, UK*

Accepted XXX. Received YYY; in original form ZZZ

ABSTRACT

The results of high-resolution spectral-line observations of dense molecular gas are presented towards the nuclear region of the type 2 Seyfert galaxy NGC 1068. MERLIN observations of the 22 GHz H₂O maser were made for imaging the known off-nuclear maser emission at radio jet component located about 0.3" north-east of the radio nucleus in the galaxy. High angular resolution ALMA observations have spatially resolved the molecular gas emissions of HCN and HCO⁺ in this region. The off-nuclear maser spots are found to nearly overlap with a ring-like molecular gas structure and are tracing an evolving shock-like structure, which appears to be energized by interaction between the radio jet and circumnuclear medium. The scenario of the dynamic jet-ISM interaction is further supported by a systematic shift of the centroid velocities of the off-nuclear maser features over a period of 35 years. The enhanced integrated flux ratios of the HCN to HCO⁺ line emission features at component C suggest a kinetic temperature $T_k \gtrsim 300\text{K}$ and an H₂ density of $\gtrsim 10^6 \text{ cm}^{-3}$, which are conditions where water masers may be formed. The diagnostics of the masering action in this jet-ISM interaction region is exemplary for galaxies hosting off-nuclear H₂O maser emission.

Key words: galaxies: active - galaxies: individual: NGC 1068 - submillimetre: galaxies - ISM: molecules - masers

1 INTRODUCTION

Highly luminous extragalactic H₂O maser in the transition of $6_{16} - 5_{23}$ (rest frequency: 22.23508 GHz) is a useful tracer of the structure and kinematics of dense molecular gas in interaction regions in galaxies and in clouds on scales of $< \sim 1$ pc from a central engine of active galactic nuclei (AGN). Some fraction of the known H₂O megamasers exhibit spectra implying evidence for emission sub-parsec clouds embedded in an edge-on rotating disc surrounding super massive black holes using Very Long Baseline Interferometry (VLBI) at milliarcsecond (mas) angular resolution (e.g., Nakai, Inoue, & Miyoshi 1993; Haschick, Baan, & Peng 1994; Miyoshi et al. 1995; Greenhill et al. 2003; Baan et al. 2022). Some of the megamaser systems were studied by the Megamaser Cosmology Project (MCP)¹, aiming the independent and high precision measurement of the Hubble constant at a 2-3 percent accuracy by measuring the megamasers hosting the "clean masering disk" systems, as in NGC4258, in the Hubble flow

with VLBI mapping and spectral monitoring. (e.g., Reid et al. 2009; Gao et al. 2016; Pesce et al. 2020).

Many of the H₂O megamasers are associated with the radio continuum emission structures resulting from nuclear radio jets, jet-cloud interaction regions or outflows such as TXFS 2226-184, NGC 1052, Mrk 348, and Centaurus A (e.g., Koeke-moer et al. 1995; Claussen et al. 1998; Peck et al. 2003; Kamenno et al. 2005; Ott et al. 2013; Surcis, Tarchi, & Castangia 2020). These four objects stand out from the other megamasers on the basis of their line profiles. The spectral line profiles of non-nuclear H₂O megamasers consist of single, broad and, relatively smooth emission profiles (FWHM ~ 100 – 200 km s^{-1}) and are different from profiles found in nuclear masers that consist of narrow components or "high-velocity" components with line-widths of a few to $\sim 10 \text{ km s}^{-1}$ spread over much wider velocity ranges of ~ 100 – 1000 km s^{-1} . These non-nuclear masers arise through the shock excitation of ambient gas in circumnuclear regions of galaxies. The masers are associated with the radio continuum emission that believed to be coincident with the nucleus.

Sub-millimetre (sub-mm) telescopes such as Atacama Large millimetre/sub-millimetre Array (ALMA) have opened

* E-mail: yhagiwara@toyo.jp (YH)

¹ <https://safe.nrao.edu/wiki/bin/view/Main/MegamaserCosmologyProject>, 2020-06-15, Jim Braatz

the possibility to make imaging studies of (sub-)millimetre masers such as H₂O maser in the transitions of 3₁₃–2₂₀ (rest frequency: 183.308 GHz) and 10₂₉–9₃₆ (rest frequency: 321.226 GHz) at high angular resolution to ~ 20 milliarcsecond (mas), which may serve to diagnose the masing processes in H₂O megamaser sources (e.g., [Humphreys et al. 2005](#); [Hagiwara et al. 2013, 2021](#)). The detection of thermally excited molecules such as HCN and HCO⁺ are also reported in these megamaser host galaxies at higher transitions at sub-millimetre wavelengths.

The galaxy NGC 1068 is a prototypical type 2 Seyfert galaxy hosting an active nucleus obscured by a torus in which broad optical emission lines are seen in polarized optical spectra (e.g. [Antonucci & Miller 1985](#)). The galaxy has been investigated extensively at all wavelengths, revealing that various species of molecular gas are abundant in the circumnuclear region, and spiral arms in the galaxy and abundant dense molecular gases related to star-forming activity are in the starburst ring (e.g. [Takano et al. 2014](#); [García-Burillo et al. 2019](#); [Sánchez-García et al. 2022](#)). NGC 1068 hosts a nearly one-sided radio jet that may be qualified as a Compact Symmetric Object and luminous and variable 22 GHz H₂O maser emission has been detected to be superposed on the radio core-jet structure at lower frequencies (e.g. [Gallimore et al. 2001](#); [Gallimore, Baum, & O’Dea 2004](#)). Sub-mm H₂O maser action in the 183 and 321 GHz transitions towards the centre of the galaxy has not yet been detected using ALMA ([Hagiwara et al. 2016](#); [Pesce, Braatz, & Impellizzeri 2016](#); [Pesce et al. 2023](#)). Very long baseline interferometry (VLBI) observations have revealed that the prominent 22 GHz H₂O maser features in NGC 1068 covering a frequency range from $V_{\text{LSR}} = 800 - 1500 \text{ km s}^{-1}$ are distributed along a linear ~ 1 pc region and originated in an edge-on ($i > 80^\circ$) molecular gas disc in the nuclear region of the galaxy (e.g. [Greenhill et al. 1996](#); [Gallimore et al. 2001](#)).

Recent sub-mm mapping observations of thermally-excited molecular emission lines in the galaxy using ALMA revealed that a parsec-scale torus structure, that surrounds the nuclear region, does not have the simple axisymmetric structure expected in the unified theory (e.g. [Impellizzeri et al. 2019](#); [Imanishi et al. 2018, 2020](#)).

[Gallimore et al. \(1996\)](#) reported the presence of H₂O maser towards radio jet component C (hereafter the “off-nuclear maser”), which is located about 0.3 arcsecond (~ 20 pc) north-east from the component S1. The off-nuclear maser is peaked at $V_{\text{LSR}} = 984.1 \text{ km s}^{-1}$ ([Gallimore et al. 2001](#)), which is blueshifted $\sim 140 \text{ km s}^{-1}$ with respect to the systemic velocity of $V_{\text{LSR}} = 1123 \pm 4 \text{ km s}^{-1}$, estimated from CO emission ([Nakai et al. 1995](#)). This off-nuclear maser region traces shocked dense molecular gas coinciding with the radio jet component C, where the jet interacts with the local interstellar medium (ISM) in the galaxy ([Gallimore et al. 1996](#)). Off-nuclear masers will thus provide additional diagnostics of the circumnuclear environment of the AGN.

Following-up the earlier studies using VLBI for clarifying the origin of the off-nuclear H₂O maser in the galaxy is of great interest with different angular resolution and different dense molecular gases at higher frequencies. In this article, the results of high-resolution mapping of 22 GHz H₂O maser and HCN and HCO⁺ thermal molecular lines in NGC 1068 using MERLIN and ALMA are presented in order to under-

stand kinematics and conditions of gas in the circumnuclear region of the galaxy.

Throughout this article, cosmological parameters of $H_0 = 67.8 \text{ km s}^{-1} \text{ Mpc}^{-1}$, $\Omega_{\text{vacuum}} = 0.692$, and $\Omega_{\text{matter}} = 0.308$ are adopted. The luminosity distance to NGC 1068 is therefore 13.5 Mpc, and 1 arcsec corresponds to ~ 65 pc in linear scale.

2 OBSERVATIONS AND DATA REDUCTION

2.1 MERLIN Observations and Data Reduction

Spectral-line observations at 22 GHz with the five telescopes of Multi-Element Radio-Linked Interferometer Network (MERLIN)², including the Mark 2 telescope. The observations of NGC 1068 were carried out over periods of 6-7 April in 2002 for ~ 16 hours in total. Phase-tracking position for NGC 1068 was RA 02^h42^m40.711^s, Dec. -00°00′47.810″ (J2000). In our observations, a single IF band of 16 MHz width with opposite circular polarizations divided to 64 spectral channels, yielding a frequency resolution ($\Delta\nu$) of 250 kHz (or 3.4 km s^{-1}) was centred at the one frequency setting and changed to other two frequency settings by shifting centre frequency during observations. Using this frequency configuration, we obtained three IF center frequencies, centred at $V_{\text{LSR}} = 597, 899, \text{ and } 1092 \text{ km s}^{-1}$. The resultant velocity coverages are $V_{\text{LSR}} = 490 - 705, 790 - 1005, \text{ and } 985 - 1195 \text{ km s}^{-1}$. The velocity range of $V_{\text{LSR}} = 705 - 790 \text{ km s}^{-1}$ was not covered. Phase-referencing observations were conducted at each frequency set, using a phase-referencing source 0237-027, an ICRF source (RA 02^h39^m45^s.4723, Dec. -02°34′40.913″ (J2000)). In earlier MERLIN observations, the position used for 0237-027 in J2000 is RA = 02^h39^m45^s.47226, Dec. = -02°34′40.″8984 (± 10 mas) ([Muxlow et al. 1996](#)). Note that the differences of these positions are well within the MERLIN synthesized beam. The observations were executed in a sequence of 6 min scans with cycling interval of 250 sec for NGC 1068 and 70 sec for 0237-027.

Amplitude and bandpass calibration were performed by observations of 3C 286 and 3C 273. Data analysis was conducted using the NRAO Astronomical Image Processing Software (AIPS) ([van Moorsel, Kembal, & Greisen 1996](#)). After initial calibration and data editing, the phase reference source 0237-027 was self-calibrated, and the phase solutions obtained from the phase reference source were applied to all IFs containing line emission. In order to make a continuum map, spectral channels without line-emission were averaged. Thus, imaging and CLEANING of the continuum emission was done separately.

The synthesized beam sizes (natural-weighting) used in the CLEAN deconvolution are $0.043'' \times 0.021''$ in the position angle (P.A.) of 57° , and the resultant rms noise level per a spectral channel ($\Delta\nu = 250 \text{ kHz}$) was about 5-6 mJy

² MERLIN is operated by the University of Manchester as a National Facility of the Science and Technology Facilities Council (STFC), and is available for use on a peer-review basis, with observing proposals dealt with by the Panel for Allocation of Telescope Time (PATT). The National Facility also hosts Jodrell Bank Observatory’s VLBI participation, linking telescopes across Europe.

beam⁻¹ (A 0.02 arcsec synthesized beam corresponds to 1.3 pc at the galaxy.). The rms noise level of a line-emission-free map made by averaging line-emission-free channels was ~ 2 mJy beam⁻¹. In this article, the velocities are calculated with respect to the Local Standard of Rest (LSR). Imaging of the calibrated data was conducted with the AIPS.

2.2 ALMA Data and Data Reduction

For analysis of the thermally-excited molecular lines and the sub-millimeter continuum, we used data of ALMA band 6 (211–275 GHz) observations (Project: 2016.1.00052.S, PI: M.Imanishi) conducted at higher spatial resolution. The observations were made from 2016 October to 2017 September. For these Cycle 4 observations, 40–44 12 m telescopes were used as a hybrid configuration with baselines ranging from 17 to 7552 m. This configuration results in a largest recoverable scale of $\sim 1.3''$ for extended emission and an angular resolution of $0.02''$. In this analysis, two 1.875 GHz wide spectral windows were used to cover HCO⁺ ($J=3-2$) and HCN ($J=3-2$) emission lines at 267.558 GHz and 265.886 GHz, respectively. More details of the observations, calibrations, and data analysis are described in (Imanishi et al. 2018). We analyzed HCO⁺ ($J=4-3$) emission line data at 356.734 GHz (Project: 2016.1.00232.S) obtained from the ALMA Science Archive. The observation was conducted on 2016 September 8.

Imaging of the calibrated data was carried out using the Common Astronomy Software Applications (CASA)³ (CASA Team et al. 2022). The continuum emission of the galaxy was subtracted from the calibrated spectral line visibility cubes using line-free channels prior to CLEAN deconvolution of line emission. The emission lines were separated out from the continuum emission. Imaging was performed using CASA with Briggs weighting (robust=0.5). The resultant synthesized beam size in the CLEAN is $0.03''-0.07''$.

2.3 Effelsberg Observations

22 GHz H_2O maser spectrum of the galaxies was obtained using Max-Planck Institute 100-m telescope at Effelsberg. The half-power beam width of the 100-m was $\sim 40''$ at 22 GHz. The pointing calibration was made by observing nearby strong continuum sources every 1 to 2 hours, yielding a pointing accuracy of better than $\sim 5''$. Observations of the maser were conducted using a 22 GHz-band receiver with a 300 MHz bandwidth, 65536 spectral channels, and dual polarization from September 24 to 26 2022 at a spectral resolution of 4.6 kHz or 0.063 km s⁻¹. Smoothing 16–32 spectral points yields $\sim 1-2$ km s⁻¹ velocity resolution at 22 GHz. Accuracy of flux density is estimated to be $\sim 30\%$.

3 RESULTS

Figure 1 shows the 5 GHz continuum map of NGC 1068 presented in Gallimore, Baum, & O’Dea (2004), overlaid on the total intensity map of the HCO⁺ ($3-2$) emission obtained

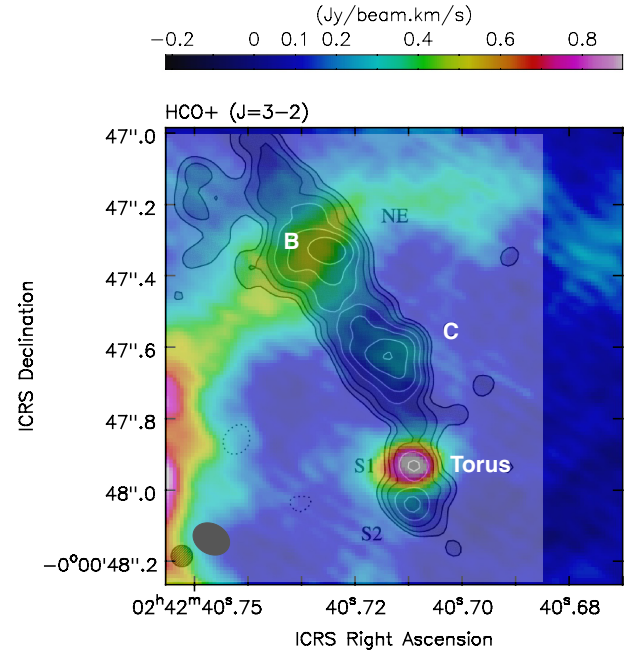


Figure 1. MERLIN 5 GHz continuum contour map by Gallimore, Baum, & O’Dea (2004) overlaid the ALMA HCO ($3-2$) total intensity map appearing in Figure 5. The four major radio components NE, C, S1, and S2 and the molecular gas torus probed by HCN and HCO⁺ (Imanishi et al. 2018) are indicated on the map. Location B, C, and S1 are HCO⁺ and HCN emission peaks defined in Figure 5. The synthesized beams of MERLIN (smaller) and ALMA (larger) are plotted at the bottom left.

by ALMA in Figure 5. Figure 2 shows 22 GHz H_2O maser spectrum towards the center of the galaxy that was taken at the Effelsberg 100-m Telescope in September 2022. Figure 3 shows the maser spectra obtained by MERLIN towards the positions of components S1 and C in the velocity range of $V_{\text{LSR}} = 800 - 997$ km s⁻¹ (the blue-shifted velocity range), $V_{\text{LSR}} = 994 - 1190$ km s⁻¹ (the systemic velocity range) towards the location of the nucleus S1, and $V_{\text{LSR}} = 800 - 1000$ km s⁻¹ towards the radio jet component C. The peak flux density of the maser is 30 mJy beam⁻¹ at $V_{\text{LSR}} = 865$ km s⁻¹ with a signal-to-noise ratio (SNR) of ~ 5 . The position of the maser at $V_{\text{LSR}} = 1162$ km s⁻¹ with a peak flux of 32 mJy beam⁻¹ near the systemic velocity is RA = $02^{\text{h}}42^{\text{m}}40.7093^{\text{s}}$, Dec. = $-00^{\circ}00'47.9479''$ (J2000). This coincides with the position of the AGN (RA = $02^{\text{h}}42^{\text{m}}40.71^{\text{s}}$, Dec. = $-00^{\circ}00'47.94''$ (J2000)) reported in Imanishi et al. (2018). The H_2O maser in the nuclear region of the galaxy was searched within the field of view of 0.768×0.768 arcsec², centred on the phase tracking centre of the galaxy and in the velocity range of $V_{\text{LSR}} = \sim 800 - 1189$ km s⁻¹. We identified possible minor peaks straddling over a few spectral channels centred at $V_{\text{LSR}} = 980.4$ km s⁻¹. The centre velocity of the peak is sim-

³ <https://casa.nrao.edu>

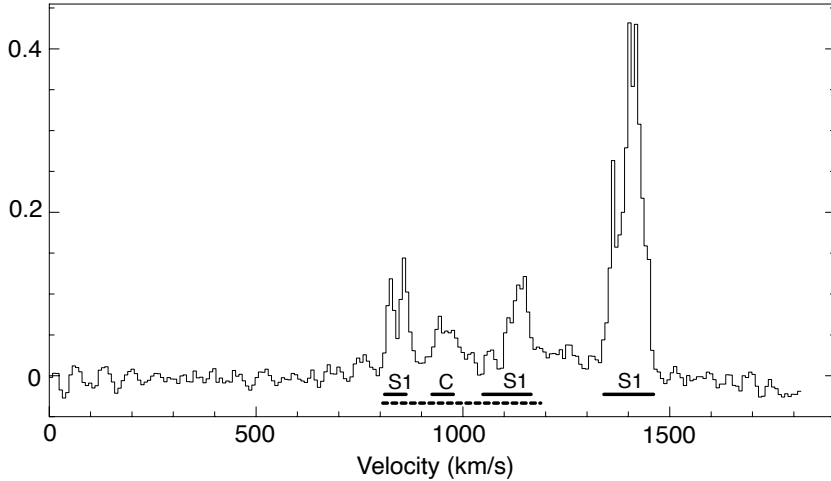


Figure 2. 22 GHz H_2O maser spectrum towards the centre of NGC 1068, obtained at the Effelsberg 100-m telescope on 24-26 September 2022. The systemic velocity of the galaxy is $V_{\text{LSR}}=1123 \text{ km s}^{-1}$ (radio, LSR) is indicated by a vertical dotted line. Short solid bars indicate the velocity ranges of the off-nuclear maser at component C and the nuclear masers at S1, respectively (Gallimore et al. 2001). A horizontal dotted line indicates the velocity range observed by the MERLIN observation in this article. Vertical axis indicates the total flux density in Jansky with the calibration error accurate to about 30 %.

ilar to the known off-nuclear maser emission at $V=984.1 \pm 1.2 \text{ km s}^{-1}$ (Gallimore et al. 2001). The position of the off-nuclear maser is $\text{RA} = 02^{\text{h}}42^{\text{m}}40.714^{\text{s}}$, $\text{Dec.} = -00^{\circ}00'47.653''$ (J2000), which is located near the radio continuum source C ($\text{RA} = 02^{\text{h}}42^{\text{m}}40.715^{\text{s}}$, $\text{Dec.} = -00^{\circ}00'47.636''$ (J2000)) (Muxlow et al. 1996). Thus, the off-nuclear maser emission is tentatively found at C, despite the fact that the detection level is $\sim 2-3\sigma$. The upper limit of the isotropic maser luminosity is estimated to be $\sim 0.1 L_{\odot}$.

The coordinates of the nuclear component at 5 GHz and the masers are listed in table 1: A mean position of the detected masers in the blue-shifted and systemic velocity range is $\text{RA} = 02^{\text{h}}42^{\text{m}}40.7087^{\text{s}}$, $\text{Dec.} = -00^{\circ}00'47.949''$ (J2000). Therefore, the positions of the masers in the blue-shifted and systemic velocity range are all confined within $\approx 0.02''$ (20 mas) from the mean position, consistent with the results of earlier observations.

Fig. 4 displays the centre positions of the nuclear masers detected in an SNR of $\gtrsim 4$ and a tentative position of the off-nuclear maser. In this figure, the nuclear maser positions are plotted also as an inset with uncertainties denoted by error bars. These nuclear maser features are peaked at $V_{\text{LSR}}=800, 861, \text{ and } 865 \text{ km s}^{-1}$ in the blue-shifted velocity range and $V_{\text{LSR}}=1068, 1105, \text{ and } 1189 \text{ km s}^{-1}$ in the systemic velocity range. All the detected masers remain unresolved at the angular resolution of ~ 20 milliarcsecond (mas), or $\sim 1.3 \text{ pc}$. Considering the position error of the calibrator source (~ 5 mas), half the synthesized beam divided by SNR (~ 4 mas), the baseline errors (~ 10 mas), and an error caused by an offset between the target and phase-reference source, positional accuracy is estimated to be ~ 15 mas. In our observations, no 22 GHz continuum has been detected to a 3σ rms noise of \sim

6 mJy beam^{-1} , making it difficult to compare precisely the locations of each maser spot and continuum components in the nuclear region of the galaxy.

Fig. 5 displays the velocity-integrated line intensity (zeroth moment) maps for HCO^+ (3-2), HCO^+ (4-3), and HCN (3-2) emission and sub-millimetre (266 GHz) continuum emission is presented in Fig. 7, obtained from the identical spectral-line cube in Fig. 5.

Fig. 6 displays mean velocity (first moment) and velocity dispersion (second moment) maps in HCO^+ (3-2) and HCN (3-2) molecular lines.

Table 2 presents line intensity ratios of HCO^+ (3-2) to HCO^+ (4-3) and HCN (3-2) to HCO^+ (3-2) at locations A, B, C and, S1 appearing both in Figure 1 and Figure 4.

4 DISCUSSION

4.1 Off-nuclear maser

In our MERLIN observations, the off-nuclear H_2O maser at component C was not distinctly detected. It is likely that the flux density of the maser was weaker when observed or it was resolved out by our MERLIN synthesized beam that is by a factor of 5 smaller than that for earlier detection with the Very Large Array (VLA) (Gallimore et al. 1996). However, the latter is less likely since the masers lying in the blue-shifted and systemic velocity ranges were detected in our MERLIN maps. Moreover, according to the recent research using a global VLBI network including the National Radio Astronomy Observatory (NRAO) VLBA, the phased-VLA, and the Effelsberg 100-m, which was observed on 2000 February 23-24, the H_2O masers at C were detected at an even

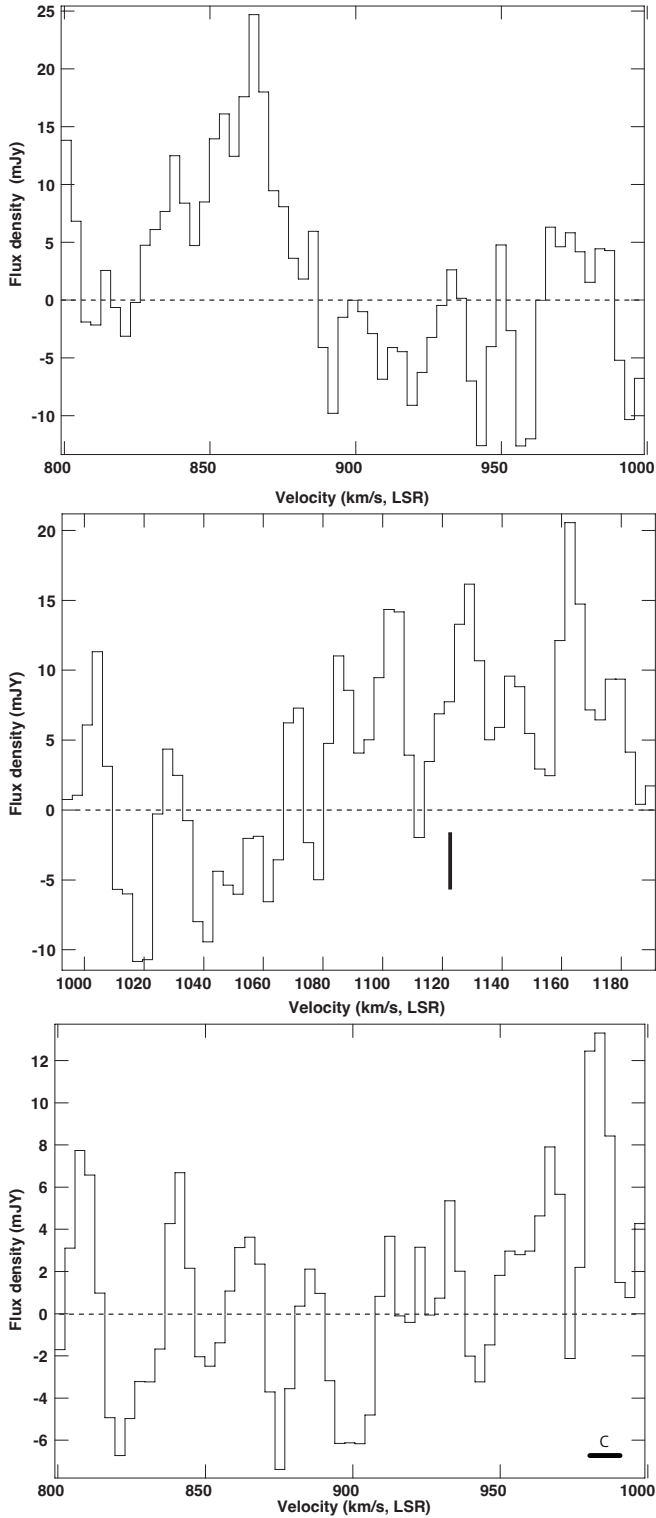


Figure 3. Spectra of the 22 GHz H_2O maser with Gaussian weighting, obtained with the MERLIN. These spectra show the nuclear masers towards S1 in the blue-shifted velocity range (top) and those in the systemic velocity range (middle). A vertical thick bar indicates the systemic velocity of the galaxy. A spectrum of H_2O maser towards the radio jet component C (bottom) shows a few minor peaks (denoted by a horizontal thick bar) centred at $V_{\text{LSR}} = 980.4 \text{ km s}^{-1}$.

Table 1. Positions of radio continuum and water maser emissions in NGC 1068.

Component	RA(02 ^h 42 ^m) (J2000)	Dec(-00°00′) (J2000)	σ_p^a
5GHz ^b			
MERLIN			
S1 (Nucleus)	40.7098 ^s	47.938 [″]	0.02 [″]
C (Jet)	40.715 ^s	47.636 [″]	0.02 [″]
VLBA			
S1 (Nucleus)	40.70907 ^s	47.9445 [″]	0.0004 [″]
C (Jet)	40.71298 ^s	47.6577 [″]	0.0005 [″]
22 GHz ^c			
S1 (Nucleus)	40.709 ^s	47.94 [″]	–
C (Jet)	40.712 ^s	47.67 [″]	–
Nuclear Water Masers			$\sim 0.01″$
$V_{\text{LSR}} = 865 \text{ km s}^{-1}$	40.709	47.94	
$= 861 \text{ km s}^{-1}$	40.708	47.96	
$= 861 \text{ km s}^{-1}$	40.708	47.96	
$= 865 \text{ km s}^{-1}$	40.708	47.94	
$= 1105 \text{ km s}^{-1}$	40.708	47.95	
$= 1162 \text{ km s}^{-1}$	40.709	47.94	
Mean position	40.708	47.94	
Off-nuclear Maser ^d			
$V_{\text{LSR}} = 980 \text{ km s}^{-1}$	40.714	47.65	

^a Position errors. The errors in Dec are larger due to the low declination of the galaxy.

^b 5-GHz nuclear continuum positions and errors are from Muxlow et al. (1996) (MERLIN) and Gallimore, Baum, & O’Dea (2004) (VLBA).

^c Measured at 22 GHz in 2015 by VLA (Mutie et al. 2023).

^d Tentative detection

Table 2. HCO^+ and HCN Line integrated intensity (in Jy km s^{-1}) ratios at Components A, B, C, and S1 are listed.

Component	HCO^+ (3-2)/(4-3)*	HCN (3-2)/ HCO^+ (3-2)
A	1.25	2.45
B	1.75	1.66
C	0.87	1.35
S1(Torus)	0.83	1.33

*The HCO^+ (4-3) emission data from Figure 5

smaller 1.3×1.0 mas angular resolution (see Figure 9)(Morishima et al. 2023). The off-nuclear masers at C were previously detected in velocities of $V_{\text{LSR}} \simeq 950\text{--}1050 \text{ km s}^{-1}$ by the VLA in 1987, and the flux density of the maser was $\sim 50 \text{ mJy}$ (Gallimore et al. 1996). If the strength of the maser was as strong as that observed by the VLA, the maser should have been clearly detected in our observations. Nevertheless, a minor 2.5σ peak at $V_{\text{LSR}} = 980.4 \text{ km s}^{-1}$ seen with MERLIN near component C in the Figures 3 and 4 would represent the location of the off-nuclear maser. The observed intensity variability of the off-nuclear maser (Gallimore et al. 2001) may indeed account for the reduced flux density of the maser at component C below $\sim 20 \text{ mJy}$ at the time of our MERLIN observations.

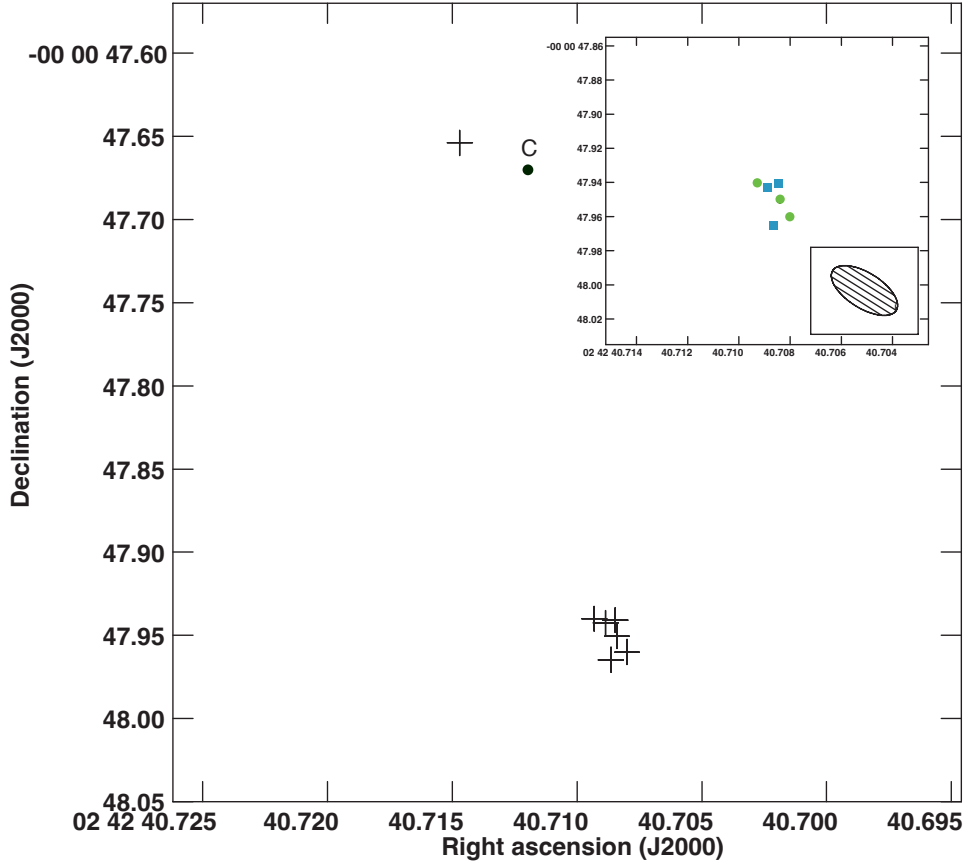


Figure 4. Centre positions of the nuclear masers and a tentative position of the off-nuclear maser, obtained by the MERLIN observation. A 22 GHz continuum peak in component C is marked by a black circle by assuming that positional uncertainties between the maser map by MERLIN and the VLA 22 GHz continuum map are negligible. The nuclear masers at the blue-shifted velocity (blue squares) and the systemic velocity (green circles) are shown also as an inset. The synthesized beam of 43.9×20.7 mas at P.A. = 58° is plotted at the bottom right corner in the inset.

4.2 Nuclear H₂O masers at the continuum nucleus (S1)

One important result in our observations is that the positions of the nuclear masers in NGC 1068 obtained at the angular resolution of ~ 20 mas have been estimated with respect to the radio nuclear component S1 in Figures 1 and 5 from earlier 5 GHz MERLIN data and has not been well established by VLBI observation. Earlier VLBI observations at 22 GHz (Greenhill et al. 1996) did not detect the nuclear continuum components, which makes astrometric registration difficult for the masers and the radio nucleus. An attempt has been made to register the relative positions of all maser emissions extending to ± 300 km s⁻¹ below systemic and the radio continuum components using VLBI data at 5 GHz (Gallimore, Baum, & O’Dea 2004). The positional uncertainties resulting from the not precisely known position of the radio nucleus S1 are comparable with those of the masers. The positions of the blueshifted masers presented in Greenhill et al. (1996) were not obtained with phase-referencing observations and their

positions were estimated relative to the brightest maser spot in the galaxy Gallimore et al. (2001). In our observations, the 22 GHz continuum was not detected and the positions of the nuclear masers have been determined with respect to the phase-referencing source used in both our observations and earlier MERLIN observations (Muxlow et al. 1996). The coordinates of the nuclear component at 5 and 22 GHz and the masers are listed in Table 1. The positions of the unresolved maser sources and the continuum nucleus at 5 GHz are co-located within the uncertainties. It should be noted that the maser positions are offset south-west or south with respect to the 5 GHz or 22 GHz continuum nucleus and some systematic position shifts between the maser spots and the 5 GHz S1 continuum source could not be removed in our data analysis. Nevertheless, we conclude that the detected blue-shifted and systemic masers arise near from the central engine of the galaxy, which is consistent with the results of earlier VLBI measurements.

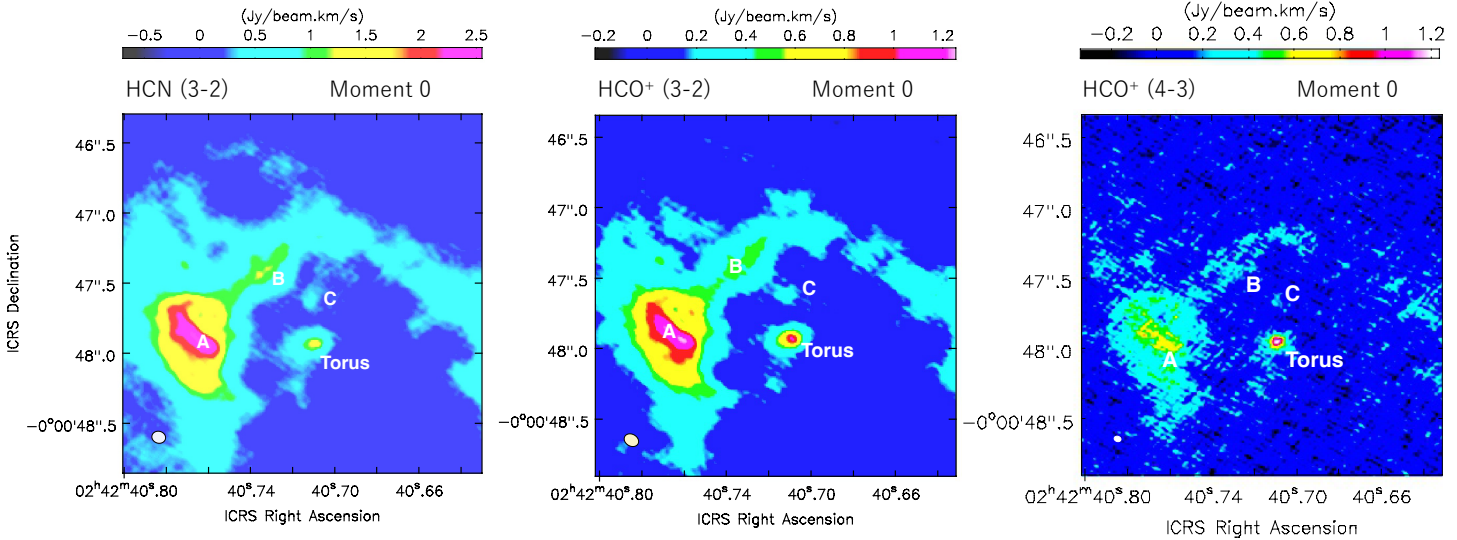


Figure 5. Color-scale total integrated intensity (zereth moment) maps of HCN and HCO^+ line emission towards the circumnuclear region of NGC 1068, presented in [Imanishi et al. \(2018\)](#). (*left:*) Zereth moment map in HCN(3–2), (*middle:*) HCO^+ (3–2) (*right:*) HCO^+ (4–3). The components A, B, C (jet and off-nuclear maser), and the torus (AGN) are marked in each panel. The synthesized beams of ALMA are plotted at bottom left.

4.3 Velocity fields in HCN and HCO^+ at C

The velocity gradients in both the HCN (3–2) and HCO^+ (3–2) emission at the radio component C have been resolved at the $\sim 0.03''$ spatial resolution of ALMA in Figure 6. As is evident in the first moment maps of Figure 6 (upper), the velocity gradients in the HCN and HCO^+ lines are spanning $V_{LSR} = \sim 1050$ to 1150 km s^{-1} and $V_{LSR} = \sim 1000$ to 1100 km s^{-1} , respectively. However, the directions of the gradients are seen to be opposite: the HCN gradient appears increasing towards north-west with red-shifted by $\sim 100 \text{ km s}^{-1}$, while the HCO^+ gradient decreases westward with blue-shifted by $\sim 100 \text{ km s}^{-1}$. The latter seems to trace outflowing materials in the local circumnuclear medium that would be with the velocity distribution of the H_2O maser emission imaged at C with milliarcsec VLBI observations as discussed below. However, there is no straightforward interpretation for this discrepancy except for the possibility that the HCN samples a much larger emission component.

Figure 6 (lower) shows the second moment maps for the two molecular emissions. In the figures, we find a high velocity dispersion region with a velocity dispersion of $\sigma_v = \sim 30$ – 50 km s^{-1} in HCN and $\sigma_v = \sim 30$ – 60 km s^{-1} in HCO^+ . The HCO^+ dispersion also shows a small gradient from nearly south to north along the assumed trajectory of the jet. The high-dispersion region in HCO^+ appears offset about $0.05''$ or 3.3 pc north of the center of C, and the high-dispersion regions in both HCN and HCO^+ are located at the edges of the line emission regions. This may indicate that the jet-ISM interaction creates a cavity that forces gases to accumulate at the edges of the gaseous regions.

4.4 Systematic velocity shift of the off-nuclear maser

Figure 8 shows time-series of the centre velocity of the off-nuclear maser at six epochs spanning from 1987 to 2022 covering a period of 35 years. To determine the centre velocity, the strongest single-peak line emission was used at each epoch, and these emission line profiles did not significantly change over the period. The values of the velocities at each epoch are taken from H_2O maser spectra in the literature listed in Fig. 8 caption. It should be noted that the flux density of the off-nuclear masers are very variable and that the maser features at C at around $V_{LSR} = \sim 980 \text{ km s}^{-1}$ were not always distinctly seen in the single-dish spectra (e.g., [Braatz et al. 2003](#)). Despite the fact that the measured velocity-shift shows such ambiguities, the plot does suggest a systematic velocity shift of about $0.85 \text{ km s}^{-1} \text{ yr}^{-1}$ in velocity in time towards the blue.

Figure 9 shows the distribution of the H_2O maser spots at component C obtained by VLBI that is superposed on the HCO^+ (3–2) emission in Figure 5, assuming that the centre of the maser distribution largely corresponds to that of the HCO^+ (3–2) ring-like structure. The maser image has been obtained with a high-sensitivity array (HSA) consisting of the VLBA, the phased-VLA, and the Effelsberg 100-m telescope on 2000 February 23–24 ([Morishima et al. 2023](#)). This figure places the maser component structure around the cavity found in HCO^+ (3–2), although there are no absolute coordinates registered for the maser distribution map presented as compared with the HCO^+ map in [Morishima et al. \(2023\)](#). Note that the 22 GHz continuum peak position of component C (marked by a cross in Figure 6) lies nearly south of the HCN and HCO^+ emission, which implies that

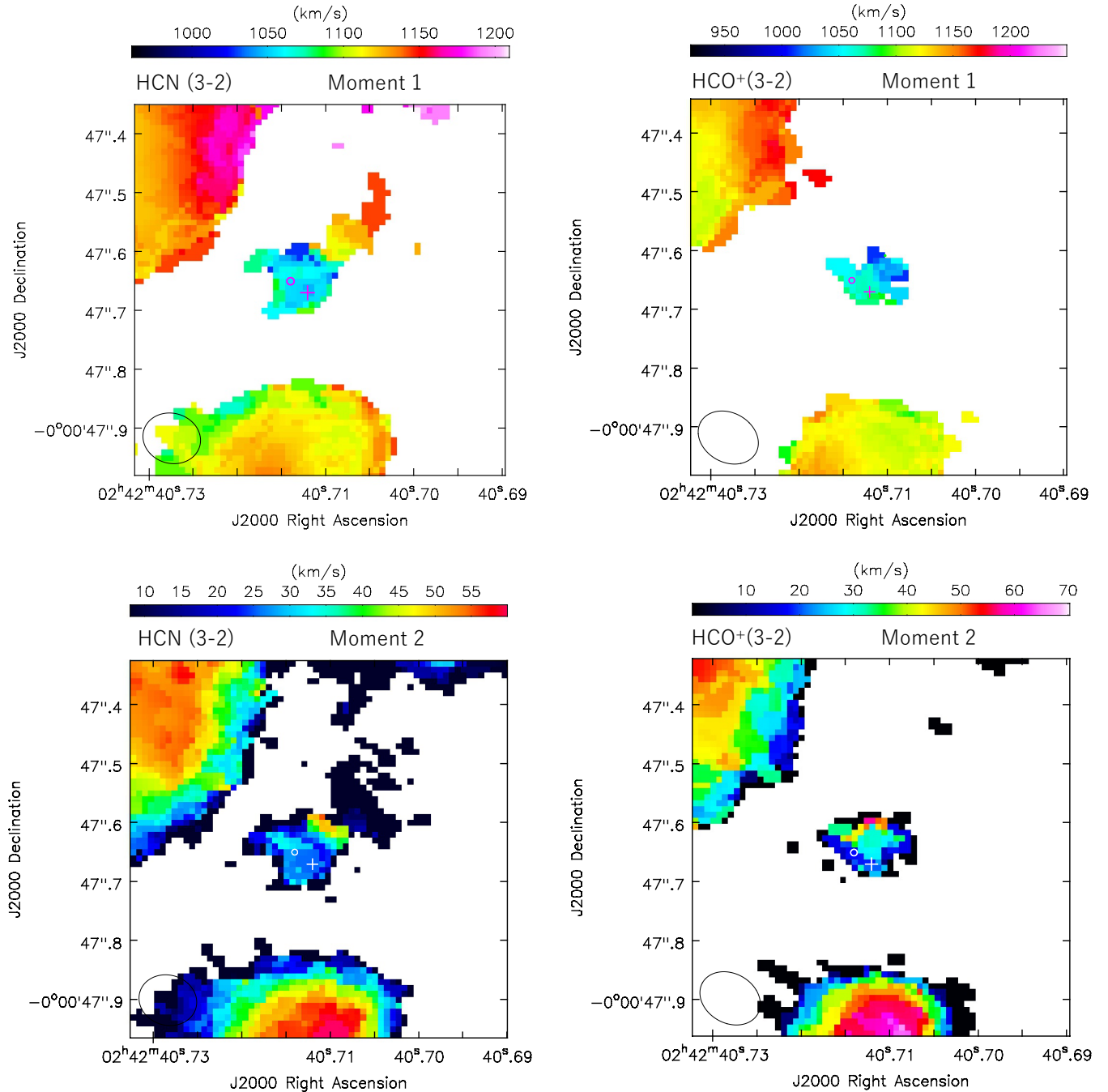


Figure 6. Moment maps in HCN (3–2) and HCO⁺ (3–2) towards the nuclear region of NGC 1068, obtained from the ALMA Cycle 4 observations. Mean velocity (first moment) maps (*upper*), and velocity dispersion (second moment) maps (*lower*) in HCN (3–2) and HCO⁺ (3–2) are presented. A 22 GHz radio continuum peak position of component C is denoted by a cross and the blue-shifted maser spot ($V_{\text{LSR}}=980 \text{ km s}^{-1}$) detected by MERLIN is marked by a circle in each panel). The synthesized beam sizes ($\sim 0.04''$) are shown in the bottom left of each panel. In these maps, the optical convention for Doppler velocities are adopted. The difference between the optical and radio velocity conventions is $\approx 5 \text{ km s}^{-1}$. The coordinates in each panel are based on the J2000 system.

the continuum peak lies at the shock front between the jet and the intervening molecular gas. It is interesting that the overall distribution of the masers at component C shows a ring-like structure with a hole or cavity at its centre, which may indicate that the presence of a strong shock in the jet-ISM interaction causes a ring-like HCO⁺ emission structure.

The blue-shifted maser features spanning $V_{\text{LSR}}=900\text{--}1100 \text{ km s}^{-1}$ depicted in Figure 9 provide evidence that the shock front between the jet and the intervening molecular gas is steadily moving towards the observer.

Very recently, the kinematics of the maser at C has been

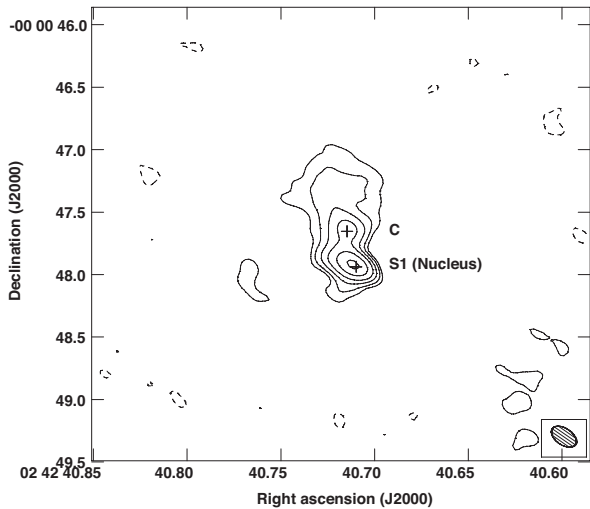


Figure 7. Sub-millimetre (266 GHz) continuum map of a nuclear region obtained by the ALMA (Imanishi et al. 2018). Contours are $-2, 3, 5, 1, 9, 15, 46 \times 1 \sigma$ value of $0.18 \text{ mJy beam}^{-1}$. The synthesized beam ($\sim 0.2'' \times 0.13''$) is at the right bottom corner. Nuclear component of S1 at 5GHz and a tentative position of the 980.4 km s^{-1} maser (Fig. 2) near the component C are marked by crosses.

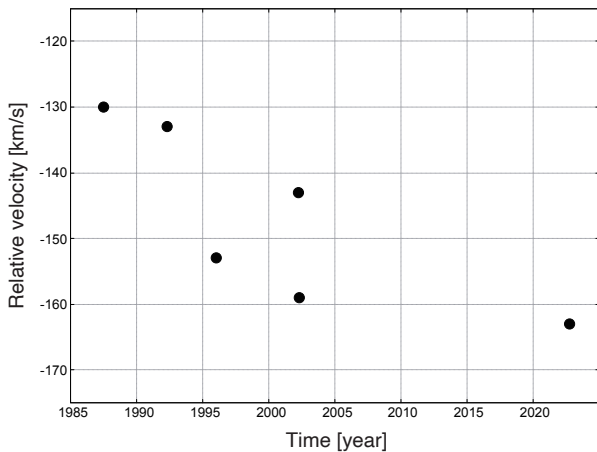


Figure 8. Time-series of the centre velocities of the off-nuclear H_2O maser obtained from 1987 to 2022. The vertical axis denotes centre velocities of the maser that are relative to the systemic velocity of NGC 1068, which are estimated from the spectra in the following references: Gallimore et al. (1996), Nakai et al. (1995), Gallimore et al. (2001), Braatz et al. (2003), and this article. The horizontal axis is time scaled in year.

revealed by the HSA observations, in which the off-nuclear masers appear to trace an expanding ring structure (Gallimore & Impellizzeri 2023) similar to the ring-like distribution of the HCO^+ emission in our data (Fig. 9). Assuming that the radius of the ring in Fig. 9 is 20 mas (1.3 pc) and the expansion speed is on the order of 100 km s^{-1} , based on the outflowing velocity shown in Fig. 8, or the outflow velocities in the shocked interstellar medium in AGN (Pounds & King 2013), the kinetic age of the ring may be estimated at ~ 12000 years. This value is similar to the 6000 years obtained from

Table 3. The relative velocities of the off-nuclear masers as a function of time are presented. The relative velocities are estimated from the difference between the systemic velocity of the galaxy and the centre velocity of the maser emission at each epoch. The value at the 1996.0 epoch is from the integrated spectra spanning 1995–1998 as stated in Gallimore et al. (2001). Data points appearing in Figure 8 are from this table.

Time (Year)	Relative Velocity (km s^{-1})	References
1987.50	-130	Gallimore et al. (1996)
1992.33	-133	Nakai et al. (1995)
1996.0	-152.9	Gallimore et al. (2001)
2002.26	-143	This article (Fig.3)
2002.32	-159	Braatz et al. (2003)
2022.76	-163	This article (Fig.2)

the Expanding Ring Model presented in Gallimore & Impellizzeri (2023). Moreover, the positions of the masers are displaced ~ 5 mas south of the 5 GHz continuum peak at C in the new HSA data, and the blue-shifted maser spot (Fig. 4) is displaced ~ 2 mas east of the 22 GHz continuum peak. Both displacements could indicate that the jet advances in the molecular medium and the maser inversion occurs at the jet shock front.

4.5 Conditions of the molecular medium at C

The observed line intensity ratios of the HCO^+ (3–2) and HCO^+ (4–3) and HCN (3–2) and HCO^+ (3–2) at component C show values that are very different from those at components A and B in Figure 1. A non-LTE radiative transfer calculation based on the RADEX program (van der Tak et al. 2007) indicates that the observed integrated flux ratio of HCO^+ (3–2) to HCO^+ (4–3) (0.87) in Table 2 can be explained by a hydrogen number density (n_{H_2}) of $\approx 10^6 \text{ cm}^{-3}$ and a kinetic temperature of $T_k = 300\text{--}500 \text{ K}$ or even warmer (Fig. 10), assuming a hydrogen column density of $10^{13}\text{--}10^{15} \text{ cm}^{-2}$ and an HCO^+ line-width of 100 km s^{-1} . These resultant values are consistent with the conditions ($T_k = 400\text{--}1500 \text{ K}$, $n_{H_2} \gtrsim 10^6 \text{ cm}^{-3}$) where water maser excitation occurs (e.g., Gray et al. 2016, 2022).

The enhanced line intensity ratio of the HCN (3–2) and HCO^+ (3–2) lines at C (1.35 in Table 2) could be explained under conditions of $T_k \geq 300 \text{ K}$, $n_{H_2} \gtrsim 10^8 \text{ cm}^{-3}$ if we take the molecular abundance ratio of HCN to HCO^+ to be about 2 (Fig. 10). Enhancement of the HCN to HCO^+ abundance ratio by a factor of three or even larger than 10 has indeed been found in nuclear AGN environments, although this may not be representative for the off-nuclear region C in NGC 1068 (e.g. Izumi et al. 2016). On the other hand, studies of the molecular abundance ratio in Ultra-luminous infrared galaxies (ULIRGs) show that the HCN to HCO^+ flux ratio also increases with changes of the HCN/ HCO^+ abundance ratio as a function of kinetic temperature and hydrogen density (Baan, Loenen, & Spaans 2010; Imanishi et al. 2023). In previous research, an elevated ratio of HCN to HCO^+ has been observed not only in the nuclear regions of AGNs and starburst galaxies but also in regions where shocks occur, such as in molecular outflow from star-forming regions (Bachiller

& Pérez Gutiérrez 1997). Mechanical heating by shocks in nuclear molecular outflows in ULIRGs could also cause the enhanced intensity ratio (Aalto et al. 2012; Izumi et al. 2013; Imanishi, Nakanishi, & Izumi 2019).

4.6 Non-detection of the sub-millimetre maser and continuum emission

Figure 7 shows that the submillimetre continuum emission at 266 GHz towards the nuclear region of the galaxy, in which the Component C is peaked north of the nuclear continuum peak S1. The Spectral Energy Distribution of the galaxy suggests that the continuum at 266 GHz is dominated by dust emission (using the photometric data points of NGC 1068 from NED) and the continuum component traces the dust emission from foreground material and heated by the obscured active nucleus.

Water maser emission at both 183 and 321 GHz would serve as a further diagnostic of the local environments but these emissions have not been detected towards the nuclear region and component C in NGC 1068 (Hagiwara et al. 2016; Pesce, Braatz, & Impellizzeri 2016). The energy level of H₂O in the 183 GHz transition ($E_u/k=205$ K) is lower than those of the 22 GHz (644 K) and 321 GHz (1862 K) transitions. Assuming that emissions in these higher transitions also result from maser amplification of the background dust emission by foreground material, recent ALMA observations at $\sim 0.6''$ angular resolution have not detected the 183 GHz maser transition at a 5σ upper limit of 37 mJy above a detected background continuum flux of 128 mJy arcsec⁻² (Pesce et al. 2023). Considering the small ratio of the upper limit of the maser flux and the continuum, low-gain amplification could result in observable maser emission.

5 SUMMARY

MERLIN observation of the 22 GHz H₂O maser emission in NGC 1068 at ~ 20 mas angular resolution has been conducted to resolve the maser and to understand the kinematics of the dense molecular gas at the shock front between the radio jet and intervening gas in the galaxy. The nuclear masers at blue-shifted and systemic velocities were detected at the location of the 22 GHz continuum nucleus of the galaxy within uncertainties. Only a minor maser peak was seen at $V_{\text{LSR}} = 980.4$ km s⁻¹ at the known off-nuclear maser position at component C, which would be consistent with the earlier results obtained by the VLA in 1983 and 1987. This maser may have faded during our observing period in 2002.

Molecular emission lines of HCO⁺ at 257 GHz and HCN at 255 GHz show an enhanced dispersion at C and weak velocity gradients in the roughly southeast to northwest direction. However, the direction of the velocity gradients of HCO⁺ and HCN is almost opposite, which may suggest that each of the emission lines probe different molecular structures. The HCO⁺ velocity gradient is largely consistent with the weak velocity gradient traced by the 22 GHz H₂O masers at component C as seen by VLBI results at mas resolution.

Analysis of published maser spectra shows that the velocity of the off-nuclear masers has shifted towards the blue during the 35 years covering six observing epochs (Fig. 8). Since component C results from the shock front between the jet and

the ambient molecular materials, this velocity drift towards the observer confirms that the jet points in front of the plane of the sky. Thus, the blue-shifted velocity of both the local HCO⁺ emission at C and the off-nuclear H₂O maser probe the jet-ISM interaction region in the nuclear outflow.

The ring-like structure imaged both at high resolution in the H₂O maser and HCO⁺ (3–2) molecular gas emission may suggest a shock-driven (cylindrical) expansion of the dense gas triggered by the heating from the decelerating shock in the radio jet. The 22 GHz off-nuclear H₂O maser components trace velocity coherent column density regions at the edges of this shock-driven expansion. The observed ring-like distribution of the line emission of HCO⁺ (3–2) superposed on the maser spots is consistent with the expanding ring model that is recently proposed in Gallimore & Impellizzeri (2023).

The non-LTE radiative transfer model calculation explains the observed molecular line intensity ratios obtained by the sub-millimetre ALMA observations. The results of our calculations using RADEX are largely consistent with conditions where 22 GHz H₂O maser excitation occurs. Thus, the data obtained from ALMA enabled us to diagnose the gas conditions required for excitation of sub-mm molecular line as well as for the H₂O maser emission.

Further observations at higher angular resolution using interferometry with VLBI and ALMA would reveal more details of the gas dynamics and conditions at component C.

ACKNOWLEDGEMENTS

The authors thank T.W.B. Muxlow and A.M.S. Richards for their help in data analysis. YH thanks H.-R. Klöckner and A. Kraus for their observing help at Effelsberg. The authors appreciate H. Sudou for providing a figure used in this article. This research was supported by Japan Society for the Promotion of Science (JSPS) Grant-in-Aid for Scientific Research (B) (Y.H.: JP15H03644) and (C) (M.I.: JP21K03632). This research has been supported by the Inoue Enryo Memorial Grant, TOYO University in Japan. WAB has been supported by the Chinese Academy of Sciences President’s International Fellowship Initiative grants 2022VMA0019 and 2023VMA0030. This research has made use of the NASA/IPAC Extragalactic Database (NED), which is funded by the National Aeronautics and Space Administration and operated by the California Institute of Technology. MERLIN is a National Facility operated by the University of Manchester at Jodrell Bank Observatory on behalf of STFC.

This article makes use of the following ALMA data: #2016.1.00052.S, 2016.1.00232.S. ALMA is a partnership of ESO (representing its member states), NSF (USA) and NINS (Japan), together with NRC (Canada) and NSC and ASIAA (Taiwan), in cooperation with the Republic of Chile. The Joint ALMA Observatory is operated by ESO, AUI/NRAO and NAOJ. Partly based on observations with the 100-m telescope of the MPIfR (Max-Planck-Institut für Radioastronomie) at Effelsberg.

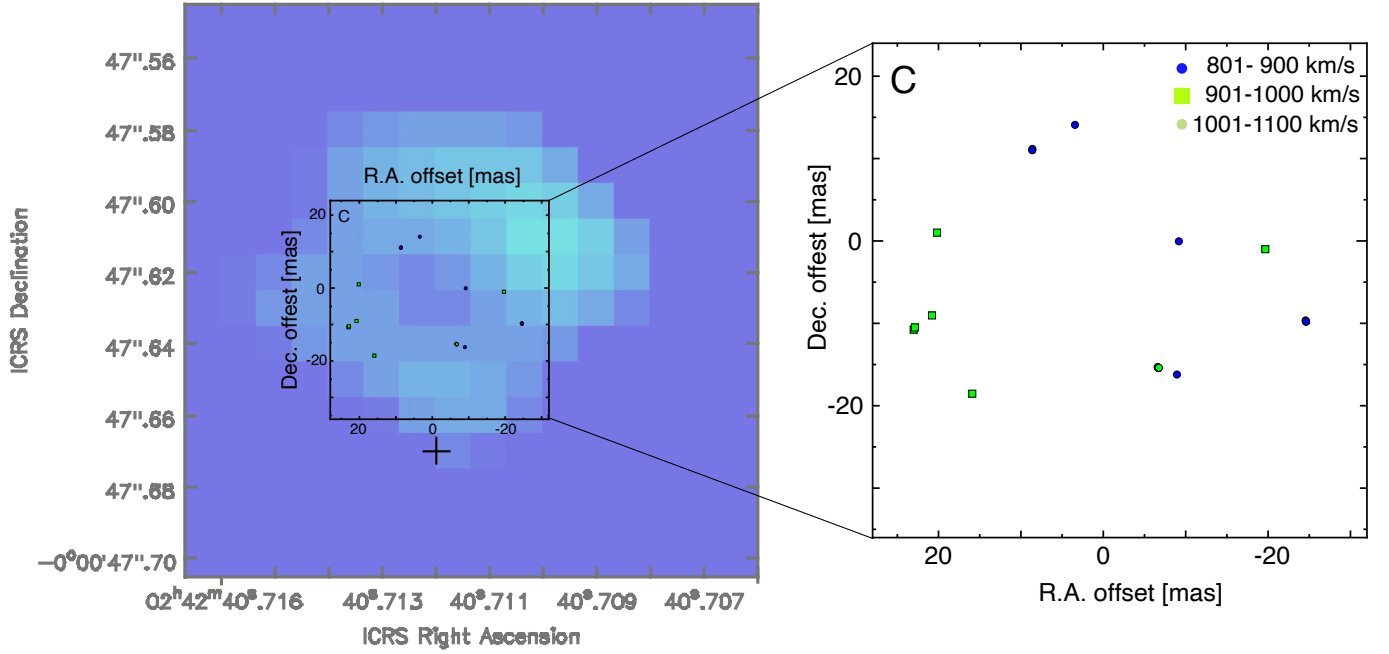


Figure 9. (*Left*.) The off-nuclear maser spots superposed on the HCO^+ (3–2) total intensity map (Figure 5) (Sudou, H., private communication). The picture assumes that the centre of the maser distribution corresponds approximately with the centre of the HCO^+ (3–2) map having a hole or a cavity in the middle. The 22 GHz radio peak position measured in component C measured by VLA is marked by a cross (Mutie, Beswick et al. in preparation). (*Right*.) Zoom-up map of the off-nuclear maser spots obtained by VLBI (Morishima et al. 2023). The $V_{LSR}=980 \text{ km s}^{-1}$ off-nuclear maser feature in Fig. 4 could be found in a group of the features lying at $V_{LSR}=901\text{--}1000 \text{ km s}^{-1}$ (green squares).

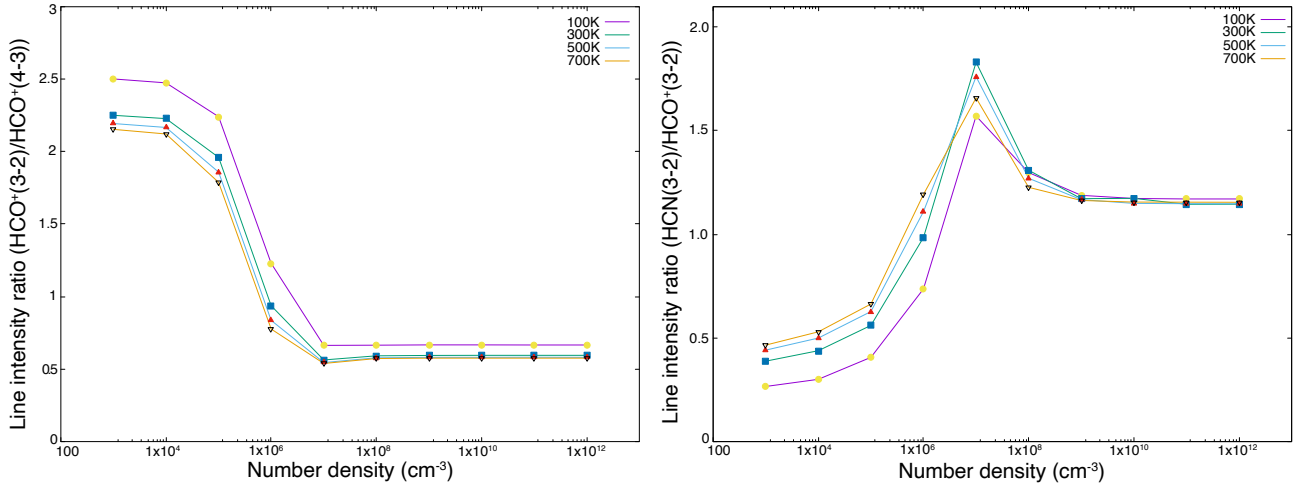


Figure 10. (*Left*.) The HCO^+ (3–2)/ HCO^+ (4–3) integrated flux density ratio as a function of the hydrogen number density (n_{H_2} in cm^{-3}) for three different kinetic temperatures: $T_{\text{kin}}=100, 300, 500,$ and 700 K , assuming the cosmic microwave background temperature ($T_{\text{bg}}=2.73 \text{ K}$), hydrogen column density ($N_{\text{H}} = 10^{13} \text{ cm}^{-2}$), and a line velocity-width ($\Delta V=100 \text{ km s}^{-1}$). (*Right*.) The HCN (3–2)/ HCO^+ (3–2) integrated flux density ratio as a function of n_{H_2} for $T_{\text{kin}}=100, 300, 500,$ and 700 K , assuming the HCN to HCO^+ molecular abundance ratio of 2. For other parameters, the same values as those in the left figure are adopted. The results in these plots are calculated using the RADEX program (van der Tak et al. 2007).

DATA AVAILABILITY

The MERLIN data used in this article will be shared on request. The molecular line data is available in the publication by [Imanishi et al. \(2020\)](#). Further data have been obtained from existing literature.

REFERENCES

- Aalto S., Garcia-Burillo S., Muller S., Winters J. M., van der Werf P., Henkel C., Costagliola F., et al., 2012, *A&A*, 537, A44. doi:10.1051/0004-6361/201117919
- Antonucci R. R. J., Miller J. S., 1985, *ApJ*, 297, 621. doi:10.1086/163559
- Baan W. A., An T., Henkel C., Imai H., Kostenko V., Sobolev A., 2022, *NatAs*, 6, 976. doi:10.1038/s41550-022-01706-y
- Baan W. A., Loenen A. F., Spaans M., 2010, *A&A*, 516, A40. doi:10.1051/0004-6361/200913207
- Bachiller R., Pérez Gutiérrez M., 1997, *ApJL*, 487, L93. doi:10.1086/310877
- Braatz J. A., Wilson A. S., Henkel C., Gough R., Sinclair M., 2003, *ApJS*, 146, 249. doi:10.1086/374417
- CASA Team, Bean B., Bhatnagar S., Castro S., Donovan Meyer J., Emonts B., Garcia E., et al., 2022, *PASP*, 134, 114501. doi:10.1088/1538-3873/ac9642
- Claussen M. J., Heiligman G. M., Lo K. Y., 1984, *Natur*, 310, 298. doi:10.1038/310298a0
- Claussen M. J., Diamond P. J., Braatz J. A., Wilson A. S., Henkel C., 1998, *ApJL*, 500, L129. doi:10.1086/311405
- Claussen M. J., Lo K.-Y., 1986, *ApJ*, 308, 592. doi:10.3847/2041-8205/829/1/L7
- Elitzur M., Hollenbach D. J., McKee C. F., 1989, *ApJ*, 346, 983. doi:10.1086/168080
- Gallimore J. F., Impellizzeri C. M. V., 2023, *ApJ*, 951, 109. doi:10.3847/1538-4357/acd846
- Gallimore J. F., Elitzur M., Maiolino R., Marconi A., O’Dea C. P., Lutz D., Baum S. A., et al., 2016, *ApJL*, 829, L7.
- Gallimore J. F., Baum S. A., O’Dea C. P., 2004, *ApJ*, 613, 794. doi:10.1086/423167
- Gallimore J. F., Henkel C., Baum S. A., Glass I. S., Claussen M. J., Prieto M. A., Von Kap-herr A., 2001, *ApJ*, 556, 694. doi:10.1086/321616
- Gallimore J. F., Baum S. A., O’Dea C. P., Brinks E., Pedlar A., 1996, *ApJ*, 462, 740. doi:10.1051/0004-6361/201936606
- Gao F., Braatz J. A., Reid M. J., Lo K. Y., Condon J. J., Henkel C., Kuo C. Y., et al., 2016, *ApJ*, 817, 128. doi:10.3847/0004-637X/817/2/128
- García-Burillo S., Combes F., Ramos Almeida C., Usero A., Alonso-Herrero A., Hunt L. K., Rouan D., et al., 2019, *A&A*, 632, A61. doi:10.1086/310346
- Gray M. D., Etoke S., Richards A. M. S., Pimpanuwat B., 2022, *MNRAS*, 513, 1354. doi:10.1093/mnras/stac854
- Gray M. D., Baudry A., Richards A. M. S., Humphreys E. M. L., Sobolev A. M., Yates J. A., 2016, *MNRAS*, 456, 374. doi:10.1093/mnras/stv2437
- Greenhill L. J., Booth R. S., Ellingsen S. P., Herrnstein J. R., Jauncey D. L., McCulloch P. M., Moran J. M., et al., 2003, *ApJ*, 590, 162. doi:10.1086/374862
- Greenhill L. J., Gwinn C. R., Antonucci R., Barvainis R., 1996, *ApJL*, 472, L21. doi:10.1086/177187
- Hagiwara Y., Horiuchi S., Imanishi M., Edwards P. G., 2021, *ApJ*, 923, 251. doi:10.3847/1538-4357/ac3089
- Hagiwara Y., Horiuchi S., Doi A., Miyoshi M., Edwards P. G., 2016, *ApJ*, 827, 69. doi:10.3847/0004-637X/827/1/69
- Hagiwara Y., Miyoshi M., Doi A., Horiuchi S., 2013, *ApJL*, 768, L38. doi:10.1088/2041-8205/768/2/L38
- Haschick A. D., Baan W. A., Peng E. W., 1994, *ApJL*, 437, L35. doi:10.1086/187676
- Herrnstein J. R., Moran J. M., Greenhill L. J., Diamond P. J., Inoue M., Nakai N., Miyoshi M., et al., 1999, *Natur*, 400, 539. doi:10.1038/22972
- Humphreys E. M. L., Vlemmings W. H. T., Impellizzeri C. M. V., Galametz M., Olberg M., Conway J. E., Belitsky V., et al., 2016, *A&A*, 592, L13. doi:10.1051/0004-6361/201629168
- Humphreys E. M. L., Greenhill L. J., Reid M. J., Beuther H.,

- Moran J. M., Gurwell M., Wilner D. J., et al., 2005, *ApJL*, 634, L133. doi:10.3847/1538-4357/abaf50
- Imanishi M., Baba S., Nakanishi K., Izumi T., 2023, *ApJ*, 950, 75. doi:10.3847/1538-4357/acc388
- Imanishi M., Nguyen D. D., Wada K., Hagiwara Y., Iguchi S., Izumi T., Kawakatu N., et al., 2020, *ApJ*, 902, 99. doi:10.1093/mnrasl/slab006
- Imanishi M., Nakanishi K., Izumi T., 2019, *ApJS*, 241, 19. doi:10.3847/1538-4365/ab05b9
- Imanishi M., Nakanishi K., Izumi T., Wada K., 2018, *ApJL*, 853, L25. doi:10.3847/2041-8213/aaa8df
- Impellizzeri C. M. V., Gallimore J. F., Baum S. A., Elitzur M., Davies R., Lutz D., Maiolino R., et al., 2019, *ApJL*, 884, L28.
- Izumi T., Kohno K., Aalto S., Espada D., Fathi K., Harada N., Hatsukade B., et al., 2016, *ApJ*, 818, 42. doi:10.3847/0004-637X/818/1/42
- Izumi T., Kohno K., Martín S., Espada D., Harada N., Matsushita S., Hsieh P.-Y., et al., 2013, *PASJ*, 65, 100. doi:10.1093/pasj/65.5.100
- Kameno S., Nakai N., Sawada-Satoh S., Sato N., Haba A., 2005, *ApJ*, 620, 145. doi:10.1086/426936
- Koekemoer A. M., Henkel C., Greenhill L. J., Dey A., van Breugel W., Codella C., Antonucci R., 1995, *Natur*, 378, 697. doi:10.1038/378697a0
- Maloney P. R., 2002, *PASA*, 19, 401. doi:10.1071/AS01100
- Miyoshi M., Moran J., Herrnstein J., Greenhill L., Nakai N., Diamond P., Inoue M., 1995, *Natur*, 373, 127. doi:10.1038/373127a0
- Morishima Y., Sudou H., Yamauchi A., Taniguchi Y., Nakai N., 2023, *PASJ*, 75, 71. doi:10.1093/pasj/psac092
- Mutic I. M., Williams-Baldwin D., Beswick R. J., Bempong-Manful E. K., Baki P. O., Muxlow T. W. B., Gallimore J. F., et al., 2023, *arXiv*, arXiv:2312.09722. doi:10.48550/arXiv.2312.09722
- Muxlow T. W. B., Pedlar A., Holloway A. J., Gallimore J. F., Antonucci R. R. J., 1996, *MNRAS*, 278, 854. doi:10.1093/mnras/278.3.854
- Nakai N., Inoue M., Miyoshi M., 1993, *Natur*, 361, 45.
- Nakai N., Inoue M., Miyazawa K., Miyoshi M., Hall P., 1995, *PASJ*, 47, 771
- Ott J., Meier D. S., McCoy M., Peck A., Impellizzeri V., Brunthaler A., Walter F., et al., 2013, *ApJL*, 771, L41. doi:10.1088/2041-8205/771/2/L41
- Peck A. B., Henkel C., Ulvestad J. S., Brunthaler A., Falcke H., Elitzur M., Menten K. M., et al., 2003, *ApJ*, 590, 149. doi:10.1086/374924
- Pesce D. W., Braatz J. A., Impellizzeri C. M. V., 2016, *ApJ*, 827, 68. doi:10.3847/0004-637X/827/1/68
- Pounds K. A., King A. R., 2013, *MNRAS*, 433, 1369. doi:10.1093/mnras/stt807
- Pesce D. W., Braatz J. A., Reid M. J., Riess A. G., Scolnic D., Condon J. J., Gao F., et al., 2020, *ApJL*, 891, L1. doi:10.3847/2041-8213/ab75f0
- Pesce D. W., Braatz J. A., Henkel C., Humphreys E. M. L., Impellizzeri C. M. V., Kuo C.-Y., 2023, *ApJ*, 948, 134. doi:10.3847/1538-4357/acc57a
- Reid M. J., Braatz J. A., Condon J. J., Greenhill L. J., Henkel C., Lo K. Y., 2009, *ApJ*, 695, 287. doi:10.1088/0004-637X/695/1/287
- Sánchez-García M., García-Burillo S., Pereira-Santaella M., Colina L., Usero A., Querejeta M., Alonso-Herrero A., et al., 2022, *A&A*, 660, A83. doi:10.1051/0004-6361/202142396
- Surcis G., Tarchi A., Castangia P., 2020, *A&A*, 637, A57. doi:10.1051/0004-6361/201937380
- Takano, S., Nakajima, T., Kohno, K., Harada, N., Herbst, E., Tamura, Y., Izumi, T., Taniguchi, A., Tosaki, T., 2014, *PASJ*, 66, 7514
- van der Tak F. F. S., Black J. H., Schöier F. L., Jansen D. J., van Dishoeck E. F., 2007, *A&A*, 468, 627. doi:10.1051/0004-6361:20066820
- van Moorsel, G., Kembell, A., & Greisen, E. 1996, *Astronomical Data Analysis Software and Systems V*, 101, 37. doi:10.1038/361045a0

This paper has been typeset from a $\text{\TeX}/\text{\LaTeX}$ file prepared by the author.